Gkantou, M., Theofanous, M., Antoniou, N. and Baniotopoulos, C. (2017). Compressive behaviour of high strength steel cross-sections. Proceedings of the Institution of Civil Engineers–Structures and Buildings.

Compressive behaviour of high strength steel cross-sections

M. Gkantou[a], M. Theofanous[a], N. Antoniou[a], C. Baniotopoulos[a]

[a]University of Birmingham, Birmingham, UK

Abstract

The recent increase in the use of high strength steels in modern engineering practice necessitates a deeper understanding of their structural response. Given that high strength steel (HSS) design specifications are largely based on a limited number of test data and assumed analogies with mild strength steel, their applicability to HSS sections needs to be assessed. In this paper FE models are developed and validated against experimental data of hot-finished S460 and S690 stub columns. Parametric studies are conducted to generate a large number of structural performance data over a wide range of cross-section slendernesses and aspect ratios. On the basis of the results, the suitability of the Eurocode Class 3 limit and the effective width equations for HSS sections is assessed. Aiming to account for the element interaction effects, which are not considered in Eurocode, an effective cross-section method applicable to HSS slender sections is presented. Finally, the continuous strength method is extended to stocky S460 sections, for which overly conservative strength predictions were observed. The reliability of the proposed design methods is verified according to Annex D of EN 1990.

Keywords: High strength steel (HSS); Hollow sections; Local imperfection; Local buckling; Effective width equations; Eurocode 3; Effective cross-section method; Continuous strength method (CSM); Plate slenderness; Cross-section slenderness

Nomenclature

Latin characters

A	Cross-sectional area
A_c	Cross-sectional area of the corners
A_{eff}	Effective cross-sectional area
B	Width
$\bar{b}$	Average ratio of test (or FE) to model resistance
b_{eff}	Effective width
COV	Coefficient of variation
CSM	Continuous strength method
$c/t\varepsilon$	Slenderness of the most slender constituent plate element
E	Young's modulus
E_{sh}	Young's modulus of the strain-hardening region
$EC3$	Eurocode 3
FE	Finite element
f_{cr}	Elastic critical buckling stress
f_{csm}	CSM ultimate stress
f_u	Ultimate stress
f_y	Yield stress
HSS	High strength steel
H/B	Cross-section aspect ratio
H	Depth
k_b	Buckling coefficient in Seif and Schafer (2010)
k_c	Buckling coefficient in Eurocode
$k_{d,n}$	Design (ultimate limit state) fractile factor
N_u	Ultimate (failure) load
n	Number of tests and FE simulations
RHS	Rectangular hollow section
SHS	Square hollow section

t	Thickness
V_δ	COV of the tests and FE simulations relative to the resistance model
V_r	Combined COV incorporating both model and basic variable uncertainties

Greek characters

β	Coefficient determined in Gardner *et al.* (2010)
γ_{M0}	Partial safety factor for cross-section resistance
ε_{csm}	Strain at ultimate load according to CSM
ε_{eng}	Engineering strain
ε_u	Strain at ultimate load
ε_y	Strain at yield load
ε_{ln}^{pl}	Logarithmic plastic strain
$\bar{\lambda}_{\mathrm{cs}}$	Cross-section slenderness
$\bar{\lambda}_{\mathrm{p}}$	Plate slenderness
$\bar{\lambda}_{\mathrm{w}}$	Web slenderness
ρ	Reduction factor for the plate element
ρ_{cs}	Reduction factor for the cross-section
ρ_f	Reduction factor for the flange
ρ_w	Reduction factor for the web
σ_{eng}	Engineering stress
σ_{true}	True stress
ω_0	Largest measured initial geometric imperfection
ω_{DW}	Initial geometric imperfection according to Dawson & Walker

1. Introduction

Advances in production technology of high strength steels (HSS) have allowed HSS with improved ductility and weldability to be produced at a lower cost, thereby rendering HSS an attractive material for structural applications. The enhanced material strength generally leads to smaller section sizes, thus resulting in lighter, more elegant structures, reduced transportation and erection costs and reduced carbon footprint with profound sustainability benefits. In order to maximise the potential benefits of HSS and increase the usage in the construction industry, appropriate design guidance in line with the observed structural response needs to be available. In Europe the design of high strength steel (i.e. steels with a yield strength higher than 460 N/mm^2 up to 700 N/mm^2) structures is covered by EN 1993-1-12 (2007), which refers back to 1993-1-1 (2005) for most design checks, but also specifies additional design rules to account for the reduced ductility and strain-hardening characteristics of such steels. Similarly, other structural steel codes (ANSI/AISC 360-10, 2010; AISI S100, 2012; AS 4100-A1, 2012) have incorporated the use of HSS within their guidance. Given that HSS design provisions are largely based on test data for mild steel and the recommended rules and methods for HSS are identical to those for normal strength steel, further investigation on the applicability of such design specifications to HSS is required.

Numerous experimental and numerical programmes have been conducted in order to evaluate the structural response of HSS at cross-sectional and member level. The investigation of the cross-sectional response through the execution of stub column tests, which is the focus of the current study, dates back to 1966 when Nishino *et al.* (1966) tested stub columns built-up from welded A514 plates ($f_y \approx 690\ N/mm^2$) and compared their response to that of their normal strength steel counterparts, whilst two decades later the local buckling of sections comprising HSS plates was studied by Usami and Fukumoto (1984). The applicability of the Australian yield slenderness limit (i.e. transition limit from fully effective sections to sections with reduced effectiveness) to HSS sections was studied by Rasmussen and Hancock (1992), who investigated the response of BISALLOY 80 (f_y =690 N/mm^2) stub columns. Yuan (1997) tested HSS wide flange beam sections to assess the applicability of slenderness limits to HSS. Yang and Hancock (2004) performed a series of compression tests on cold-

formed G550 ($f_y = 550\ N/mm^2$) stub columns in order to evaluate the influence of the decreased strain-hardening material characteristics on the compression capacity, whereas Gao *et al*. (2009) studied the influence of the width-to-thickness ratio and the cross-section aspect ratio on the ultimate load carrying capacity of thin-walled box columns with $f_y \approx$ 745-800 N/mm^2. The local buckling response of HSA 800 ($f_u = 800\ N/mm^2$) box and I-sections was investigated by Yoo *et al.* (2013), while the results of concentric stub column tests on sections of the same material have been utilised for the assessment of Korean stability criteria (Kim *et al.*, 2014). Two more series of experimental investigations on stub columns with a nominal yield strength of 460 N/mm^2 were executed in order to evaluate the applicability of various international design codes to HSS (Zhou *et al.*, 2013b; Shi *et al.*, 2014), whilst Shi *et al.* (2016) recently studied numerically the ultimate behaviour of normal and high strength steel welded sections.

Complementing the published studies on the applicability of current design provisions to HSS sections, the present study investigates the structural behaviour of S460 and S690 hot-finished square and rectangular hollow sections and provides relevant design recommendations.

2. Numerical modelling

The general purpose FE software ABAQUS (Hibbitt *et al.*, 2010) was used for the execution of the numerical modelling described in this section. The developed finite element models were validated against the experimental results of S460 and S690 concentrically loaded stub columns reported by Wang *et al*. (2017). The validated numerical models were subsequently used for the execution of extensive parametric studies, which enabled the investigation of the structural response of HSS rectangular hollow sections with varying cross-section slendernesses and aspect ratios.

2.1. Brief description of the experimental programme

In order to study the structural response of hot-finished HSS sections in compression, a comprehensive experimental programme comprising eleven concentric stub columns was performed (Wang *et al*., 2017). The tested sections were hot-rolled seamlessly from continuously cast round

ingots and hollowed out in a piercing mill to their final section shape. The high strength in S460 sections was achieved with the normalising process, whilst in S690 with the quenching and tempering process. An initial series of coupon tests provided the material stress–strain response, which exhibited a distinct yield plateau followed by a strain-hardening range, more pronounced in S460 than S690. Typical stress–strain curves obtained from the tensile coupon tests are depicted in Figure 1. For grade S460 the average obtained values for the yield strength f_y and the ultimate tensile stress f_u were 484 N/mm^2 and 643 N/mm^2 respectively, whilst the respective average values for S690 were 764 N/mm^2 and 802 N/mm^2. Having established the material behaviour, six S460 and five S690 stub columns were concentrically loaded to failure. The nominal dimensions of the tested specimens together with a summary of the test results are given in Table 1. Further details on the measured dimensions and the fabrication process of the specimens and the experimental procedure are provided in Wang *et al*. (2017). As anticipated, the most dominant failure type was local buckling. Elephant foot failure mode, owing to the friction between the ends of the specimen and loading plates, was noticed in some stocky sections with very low imperfection magnitudes. It should be noted that all specimens failed at loads beyond their squash load.

2.2. Modelling assumptions

In line with past studies (Zhou *et al*., 2013b; Wang *et al*., 2016) which employed the four-noded doubly curved shell element S4R with reduced integration and finite membrane strains for the development of FE models capable of efficiently capturing the cross-sectional performance, this element type has been used for the development of the FE models described herein. An initial mesh convergence study revealed that an average element size equal to the thickness of the modelled component was sufficient to accurately replicate the experimentally observed structural behaviour within reasonable computational time. All degrees of freedom were restrained at both ends of the modelled stub columns except for the axial translation of the loaded end, where an incremental axial displacement was applied.

The material properties employed in the numerical models were based on the stress–strain curves recorded from the tensile flat coupon tests. An elastic-plastic model with von Mises yield criterion and isotropic hardening was adopted. Eqs. (1)-(2),

$$\sigma_{true} = \sigma_{eng}\left(1 + \varepsilon_{eng}\right) \tag{1}$$

$$\varepsilon_{ln}^{pl} = \ln\ (1 + \varepsilon_{eng}) - \frac{\sigma_{true}}{E} \tag{2}$$

where σ_{eng} and ε_{eng} are the engineering stress and strain respectively, E is the Young's modulus and σ_{true} and ε_{ln}^{pl} are the true stress and logarithmic plastic strain respectively, have been applied for the conversion of the measured engineering stress–strain curves to true stress–logarithmic plastic strain curves, before their input into the software.

Buckling is triggered in real members by the initial geometric imperfections inherently present. In order to ensure adequate replication of the experimentally observed response, the initial geometric imperfections need to be explicitly incorporated in the numerical models. In accordance with similar studies (Zhou *et al*., 2013b; Wang *et al*., 2016), an effective and easy representation of the real geometric imperfection pattern can be obtained through the incorporation of the elastic buckling mode shape corresponding to the lowest elastic critical buckling load. In addition to the shape of the initial geometric imperfections, their magnitude is of significant importance when simulating any type of buckling. In the current study the following six local imperfection magnitudes have been considered: no imperfection, $t/100$, $t/50$, $t/10$, the maximum measured imperfection ω_0 as reported by Wang *et al*. (2017) and shown in Table 1 and an imperfection amplitude proposed by Dawson and Walker (1972) and modified by Gardner and Nethercot (2004), as defined by Eq. (3),

$$\omega_{DW} = \beta\sqrt{\frac{f_y}{f_{cr}}}t \tag{3}$$

where f_y is the yield strength of the plate material, f_{cr} is the theoretical local buckling stress of the most slender constituent element of the section, t the plate thickness, and coefficient $\beta = 0.028$, as proposed for carbon steel hot-rolled rectangular hollow sections in Gardner *et al.* (2010).

In addition to the initial geometric imperfections, the residual stresses arising during the forming process may influence the ultimate structural performance of components failing by buckling. Wang *et al*. (2016) measured and reported the residual stress patterns and magnitudes for hot-finished HSS sections. The magnitudes of the recorded residual stresses were found to be 5.5% and 3.1% of the yield strength f_y for the tensile and compressive residual stresses respectively. Due to their very low magnitudes compared to the material yield strength, it was decided not to explicitly introduce residual stresses in the finite element models.

Having developed the numerical models for the concentric stub columns, a nonlinear static analysis using the modified Riks procedure and taking due account of material and geometric nonlinearities (Hibbitt *et al.*, 2010) was performed. The full load–displacement path was traced and the ultimate loads together with the corresponding end-shortenings were obtained.

2.3. Validation of the FE models

In order to ensure that the FE models can accurately predict the structural response of HSS stub columns, the experimental stiffness, ultimate load, overall response and failure mode reported by Wang *et al.* (2017) need to be accurately replicated by the FE models. To this end, the numerical load–end-shortening curves are compared with the experimental ones, as depicted in Figure 2 for SHS 90×90×3.6 in grade S460 and SHS 90×90×5.6 in grade S690. The effect of the magnitude of the initial geometric imperfection on the ultimate load and the post ultimate response can be seen in Figure 2. Typical experimental and numerical failure modes classified as local buckling and elephant foot are shown in Figure 3. The ratios of the numerical to the experimental ultimate loads ($N_{u,FE}/N_{u,Exp}$) for varying imperfection magnitudes are reported in Table 2, where a fairly accurate numerical prediction of the ultimate load capacity for all of the considered initial geometric imperfection amplitudes can be observed.

It should be noted that the present research work was part of a series of studies investigating the cross-sectional performance of S460 and S690 steel grades. Three series of experimental and numerical studies were performed: 3-point and 4-point bending tests (Wang *et al.*, 2016), eccentrically loaded

stub column tests (Gkantou *et al.*, Submitted) and concentric stub column tests. In all cases, the numerically obtained load-deformation response for six different considered imperfection magnitudes (i.e. no imperfection, ω_0, ω_{DW}, $t/100$, $t/50$, $t/10$) was compared with the experimental one. In order to maintain consistency, one imperfection magnitude able to give the best replication in all three studies was selected for the execution of the subsequent parametric studies. On the basis of the numerical to experimental comparison ratios of ultimate loads, it was shown that the imperfection magnitude able to give overall the best agreement with the experimental results was $t/50$ (i.e. $M_{u,FE}/M_{u,Exp}$ equal to 1.01 and 0.99 in 3-point and 4-point beams, respectively (Wang *et al.*, 2016) and equal to 0.98 in eccentric stub columns (Gkantou *et al.*, Submitted)). As shown in Table 2, the imperfection magnitude of $t/50$ resulted in a mean value of $N_{u,FE}/N_{u,Exp}$ equal to 0.96 with COV of 0.05, which was deemed a slightly conservative but sufficiently accurate prediction of the ultimate response of concentric stub columns and can therefore be used for the execution of parametric studies.

2.4. Parametric studies

Having validated the finite element models against the test results, thorough parametric studies were conducted to generate additional structural performance data that would allow an in-depth understanding of the cross-sectional response and a meticulous evaluation of relevant design specifications. Six cross-section aspect ratios (H/B=1.00, 1.25, 1.50, 2.00, 2.50 and 3.00) were studied in order to investigate the effect of the plate element interaction on the cross-sectional response of HSS sections. Both S460 and S690 steel grades were considered in order to study the effect of the strain-hardening material properties. Maintaining the cross-section outer dimensions and varying the cross-section thickness, cross-sections with a $c/t\varepsilon$ ratio ranging from 10 to 100 were modelled, where c is the compressed flat width, t is the plate thickness and $\varepsilon = \sqrt{235/f_y}$. In line with past studies (Gardner and Nethercot, 2004; Bock and Real, 2015; Wang *et al.*, 2016), the average material properties obtained for each steel grade from the tensile coupon tests (Wang *et al.*, 2016) were incorporated in the FE models. The length of the specimens was set equal to three times the largest cross-section dimension, thus allowing for a sufficient representation of the initial local

geometric imperfection pattern but excluding global buckling failure mode (Galambos, 1998). An imperfection magnitude of $t/50$ was introduced in the form of the lowest elastic buckling mode shape.

The failure load and the corresponding end-shortening as well as the full load–displacement path were recorded for each analysis. Typical curves of the load–end-shortening response are given in Figure 4. As anticipated, the stocky sections exhibited significant strain-hardening before reaching their ultimate load, whereas local buckling led to failure at average compressive strains within the elastic range for slender sections. Typical elastic critical buckling mode shapes and failure modes are depicted in Figure 5.

3. Analysis of the results and design recommendations

In this section, the results of the parametric studies are presented and used for the assessment of various design specifications. The suitability of the Eurocode Class 3 slenderness limit for internal elements in compression and the Eurocode effective width equations for HSS sections are initially assessed. Thereafter, the design of slender sections incorporating the effect of the element interaction is attempted by proposing an effective cross-section rather than an effective width approach. Finally, the applicability of the continuous strength method (CSM) for the design of stocky cross-sections in grade S460, which exhibit significant strain-hardening, is assessed. Appropriate design recommendations are made and new equations to make the design methods applicable to hot-finished HSS sections are proposed.

3.1. Eurocode Class 3 limit and effective width equations

Eurocode (EN 1993-1-12, 2007 referring to 1993-1-1, 2005) adopts the concept of the cross-section classification in order to treat local buckling. Comparing the width-to-thickness ratio of the constituent plate elements to the codified plate slenderness limits, a structural cross-section can be classified into four classes, with the cross-sectional response being related to the class of the most slender plate element. The codified plate slenderness limits vary depending on the stress distribution, the material properties and the boundary conditions of the assembly plate elements. Given that the

same limits with mild strength steel have been adopted for HSS, the applicability to HSS needs to be examined.

The Class 3 slenderness limit defines the transition from a fully effective (i.e. Class 1–3) to a slender (i.e. Class 4) section. Class 1–3 sections can attain their yield load capacity under pure compression, whilst Class 4 sections fail by local buckling before their squash load is reached. In order to assess the codified slenderness limit for internal elements in compression, the ultimate load capacities of the studied concentric stub columns of the two steel grades considered have been normalised by the respective squash loads (Af_y) and plotted against the $c/t\varepsilon$ slenderness of the most slender constituent plate element. The results are shown in Figure 6(a), where the current Class 3 limit of 42 is also included. As can be observed, the sections with slenderness lower than 42 fail at or beyond their squash load, showing that the codified slenderness limit is applicable to hot-finished S460 and S690 hollow sections. Moreover, for cross-sections of the same aspect ratio, the steel grade has no obvious influence on the normalised performance of slender sections which fail within the elastic range, whilst affects the response of sections in the stocky slenderness range. As can be seen, conservative strength predictions are observed for stocky sections. The latter is more pronounced for S460 sections than their S690 counterparts and is due to the Eurocode assumption of an elastic-perfectly plastic material response that ignores the strain-hardening material properties.

In order to account for the loss of effectiveness due to local buckling occurring in Class 4 sections, the traditional effective width method is employed by EN 1993-1-12 (2007). For internal elements in compression with $c/t\varepsilon > 42$, Eq. (4) is used for the estimation of the effective width (b_{eff}) (EN 1993-1-5, 2006), where ρ is the reduction factor given from Eqs. (5)-(6), $\bar{\lambda}_p$ the plate slenderness given by Eq. (7) and k_c the buckling coefficient depending on the plate's support conditions and applied stress.

$$b_{eff} = \rho\, b \tag{4}$$

$$\rho = 1.00 \; for \; \bar{\lambda}_p \leq 0.673 \tag{5}$$

$$\rho = \frac{(\bar{\lambda}_p - 0.22)}{\bar{\lambda}_p{}^2} \; for \; \bar{\lambda}_p > 0.673 \tag{6}$$

$$\bar{\lambda}_p = \frac{c}{28.4\sqrt{k_c}t\varepsilon} \tag{7}$$

Having determined the effective width of each element of the cross-section, the effective cross-sectional area (A_{eff}) is evaluated, which multiplied by the yield stress gives the cross-section compressive resistance. The buckling coefficient k_c employed in the plate slenderness formula of Eq. (7) is taken equal to 4 for internal elements in compression, assuming simply-supported edges for the plates of both square and rectangular hollow sections. However, with increasing cross-section aspect ratio, the slender webs of a rectangular hollow section, are more effectively restrained against local buckling by the shorter (hence stockier) flanges. This is neglected in current European design provisions and each plate element is treated in isolation.

For RHS with fully effective flanges (i.e. shorter faces), the actual reduction factor of the web ρ_w, as obtained from the FE results is derived from Eq. (8),

$$\rho_w = \frac{N_{u,FE} - f_y A_c - 2 f_y b_f t}{2 f_y b_w t} \tag{8}$$

where $N_{u,FE}$ is the numerical failure load of the modelled stub column, A_c is the area of the corner region which is assumed fully effective, b_f is the width of the fully effective flanges and b_w the width of the slender webs (i.e. longer faces). When both the flanges and the webs are slender, the actual reduction factor of the most slender element ρ_w can be derived on the basis of the FE failure load assuming that the ratio of the flange to the web reduction factor (ρ_f/ρ_w) is equal to the one specified in EN 1993-1-5 (2006), according to Eq. (9).

$$\rho_w = \frac{N_{u,FE} - f_y A_c}{2 f_y t (b_w + b_f \frac{\rho_f}{\rho_w})} \tag{9}$$

In Figure 6(b) the reduction factor of the most slender constituent plate element ρ_w is plotted against the corresponding slenderness $\bar{\lambda}_w$. As can be observed, even though safe predictions are achieved overall, more conservative predictions are obtained for sections with higher cross-section aspect ratios and less conservative for the square hollow sections. The same conclusion can be drawn from Table 3, where increasing aspect ratio is shown to lead consistently to more conservative strength predictions. This is clearly due to the element interaction between plated elements of dissimilar slenderness. It is worth noting that particularly for HSS, where slender sections are becoming increasingly common due to the increased material strength, it is important for the design to ensure safe but not overly conservative predictions that could reduce the benefits of adopting HSS. Hence a design approach offering consistently accurate predictions throughout a range of aspect ratios likely to occur in practice is warranted.

3.2. Effective cross-section method for slender sections

Based on the effective width equations applied to constituent plate elements of sections prone to local buckling, a method providing a reduction factor for the gross cross-sectional area has been previously proposed for slender stainless steel sections (Zhou *et al.*, 2013a; Bock *et al.*, 2015). The method, named effective cross-section method herein, expresses the reduction factor as a function of the plate slenderness $\bar{\lambda}_p$ and the cross-section aspect ratio H/B, thus allowing for the influence of the element interaction on the cross-sectional response. The method applies to both S460 and S690 slender stub columns.

Aiming to relate the cross-section reduction factor ρ_{cs} to both the plate slenderness and the cross-section aspect ratio, an equation between the numerical compressive capacities normalised by the yield load -excluding the contribution of the corner regions which are assumed not to undergo local buckling- and the slenderness $c/t\varepsilon$ of the most slender element for all Class 4 sections was derived for each aspect ratio. The cross-section reduction factor ρ_{cs} has the general form of the Winter curve and is given by Eq. (10),

$$\rho_{cs} = \frac{\bar{\lambda}_p - A}{\bar{\lambda}_p^{\,B}} = \frac{\frac{c}{28.4\sqrt{k_c}t\varepsilon} - A}{\left(\frac{c}{28.4\sqrt{k_c}t\varepsilon}\right)^B} = \frac{\frac{c}{56.8t\varepsilon} - A}{\left(\frac{c}{56.8t\varepsilon}\right)^B} \quad (10)$$

where A and B are coefficients depending on the cross-section aspect ratio H/B and k_c the buckling coefficient as defined in EN 1993-1-5 (2006). A linear regression analysis has been conducted for each of the cross-section aspect ratios considered and the A and B values were obtained. Subsequently, empirical Eqs. (11)-(12) relating the A and B coefficients to the aspect ratio H/B were determined, as shown in Figure 7(a).

$$\mathrm{A} = 0.083\,(H/B)^{-2.325} + 0.123 \quad (11)$$

$$\mathrm{B} = 0.468\,(H/B)^{-2.397} + 1.605 \quad (12)$$

Incorporating Eqs. (11)-(12) in Eq. (10), the effective cross-section curves can be derived as a function of both the cross-section aspect ratio and the slenderness $c/t\varepsilon$. As shown in Figure 7(b) and in Table 3, the proposed Eqs. (10)-(12) yield accurate strength predictions, since they are explicitly allowing for the interaction between the constituent plate elements of hot-finished hollow sections. To further evaluate the accuracy of the effective cross-section method, test data on HSS concentric stub columns collated from literature (Rasmussen and Hancock, 1992; Sakino *et al*., 2004; Im *et al*., 2005; Yoo *et al*., 2013) have been used. The results are summarised in Table 4, revealing the capability of the proposed method to predict accurate design estimations for both SHS and RHS slender cross-sections.

3.3. Continuous strength method for stocky sections

In order to obtain accurate strength predictions over the full slenderness range, a rational exploitation of the strain-hardening exhibited for sections in S460 material in the stocky slenderness region is deemed necessary. To this end, the continuous strength method (CSM) which was originally developed for stainless steel sections (Gardner, 2002) and later expanded to cover carbon steel and aluminium alloys (Gardner and Ashraf, 2006; Su *et al.*, 2014; Foster *et al.*, 2015), is extended to cover hot-finished cross-sections in S460 grade. The CSM is based on an empirical relationship between the cross-section slenderness and the strain at failure due to local buckling, which defines the so-called base curve, and assumes an elastic-linear hardening material response, thus allowing stresses in excess

of the yield stress to be taken into account when designing very stocky cross-sections. It is only applicable to sections with cross-section slenderness $\bar{\lambda}_{cs} = \sqrt{f_y/f_{cr}} \leq 0.68$ which fail at an average stress beyond their yield stress, where f_{cr} is the elastic critical buckling stress of the section. In this paper the elastic critical buckling stress of the cross-section was obtained from the expressions developed by Seif and Schafer (2010) upon execution of finite strip analysis on a large number of sections. The expressions take into account the effect of the element interaction on the elastic critical buckling stress. For hollow sections under pure compression, the equations are shown in Eqs. (13)-(14),

$$f_{cr} = k_b \frac{\pi^2 E}{12\,(1-v^2)} \left(\frac{t}{b}\right)^2 \tag{13}$$

$$k_b = 4/(h/b)^{1.7} \tag{14}$$

where E is the Young's modulus, v the Poisson's ratio, h and b the centerline depth and width of the section, t the thickness of the plate material and k_b the local buckling coefficient accounting for both boundary and loading conditions and including plate element interaction effects. Alternatively, the critical stress of the cross-section can be conservatively taken as the critical stress of its most slender plate element. Incorporating a continuous relationship between the cross-section slenderness and the cross-section deformation capacity, the cross-section compression resistance $N_{u,CSM}$ can be evaluated from Eqs. (15)-(16),

$$N_{u,CSM} = A f_{csm} = A(f_y + E_{sh}\left(\varepsilon_{csm} - \varepsilon_y\right)) \tag{15}$$

$$\frac{\varepsilon_{csm}}{\varepsilon_y} = \frac{0.25}{\bar{\lambda}_{cs}^{3.6}} \text{ but } \frac{\varepsilon_{csm}}{\varepsilon_y} < 15 \tag{16}$$

where A the cross-sectional area, ε_y the strain at yield load, f_{csm} the CSM failure stress, ε_{csm} the strain at the CSM failure load and E_{sh} the strain-hardening modulus. Thus the method does not limit the maximum attainable stress of a cross-section to the yield stress, but allows for strain-hardening exhibited by stocky sections which fail at high inelastic strains. The limit of 15 imposed on the $\varepsilon_{csm}/\varepsilon_y$ ratio relates to the ductility requirements and is in accordance with the minimum guaranteed ε_u value given in the relevant Eurocodes, EN 1993-1-1 (2005) and EN 1993-1-4 (2015) for carbon steel and stainless steel respectively. The respective value for HSS is 10 since high strength steels are

usually associated with a lower ductility (EN 1993-1-12, 2007). This limit ensures that no tensile fracture occurs when applying the CSM on flexural members. Since this paper focuses on the response of compressive members, where no tension fracture can occur, this limit is not applied herein.

In order to assess the applicability of the CSM to S460 hollow sections, the $\varepsilon_u/\varepsilon_y$ ratio, where ε_u is the strain at failure, defined as the end-shortening at failure load normalised by the initial stub column length, has been plotted against the cross-section slenderness $\bar{\lambda}_{cs}$ in Figure 8(a). The base curve given by Eq. (16) is also depicted in the same figure. The current base curve does not provide a close approximation to the obtained numerical results, presumably due to differences between the response of materials with a Ramberg-Osgood type of behaviour for which the base curve was originally developed and materials with a yield plateau. Since the base curve does not follow the obtained results closely, a least square regression analysis has been applied to the stub column results and a new base curve defined by Eq. (17) is derived. Further research is needed to support the use of this equation to other steel grades.

$$\frac{\varepsilon_{csm}}{\varepsilon_y} = \frac{0.027}{\bar{\lambda}_{cs}^{\,2.63+9.94\bar{\lambda}_{cs}}} \tag{17}$$

Having developed the base curve, a material model capable of accounting for strain-hardening is required for the implementation of the CSM. To this end, the assumption of a modest strain-hardening modulus $E_{sh} = 1/100$, as recommended by Annex C of EN 1993-1-5 (2006), is adopted. As shown in Figure 8(b), a very good approximation of the material response of S460 is achieved with the simplified bilinear model. Note that more complicated material responses including a trilinear approximation which accounted for the observed plateau led to more involved design equations without a significant improvement in the accuracy of the strength predictions. The ultimate capacities obtained from the tests (Wang *et al*., 2017) and the FE studies are normalised by the ones predicted by the CSM and plotted against the cross-section slenderness $\bar{\lambda}_{cs}$. The results are presented in Figure 8(c), where an noticeable improvement in the accuracy of the CSM strength predictions compared to the Eurocode approach can be seen. This is also shown in Table 5, where more accurate design

predictions both in terms of achieved mean values and consistency have been attained with the application of the CSM.

4. Reliability analysis

In order to assess the reliability of the proposed design methods, a statistical analysis following the provisions of Annex D EN 1990 (2002) has been carried out. In particular, the CSM method and the effective cross-section method have been statistically validated. Table 6 summarises the following key statistical parameters: the number of tests and FE simulations n, the design (ultimate limit state) fractile factor $k_{d,n}$, the average ratio of test (or FE) to model resistance based on a least squares fit to all the data $\bar{b}$, the coefficient of variation of the tests and FE simulations relative to the resistance model V_δ, the combined coefficient of variation incorporating both model and basic variable uncertainties V_r and the partial safety factor for cross-section resistance γ_{M0}. Based on the reliability analysis considerations provided in Wang *et al.* (2016), the material over-strength of HSS was taken equal to 1.135 with a COV of 0.055, whilst the COV of geometric properties was assumed equal to 0.02. The variation between the experimental and the numerical results which was found 0.052 was also considered. Performing a First Order Reliability Method (FORM) in accordance with the Eurocode target reliability requirements, the partial factors γ_{M0} were evaluated. As shown in Table 6, γ_{M0} was found to be lower than unity, indicating that the currently adopted value (i.e. γ_{M0}=1.00) could be safely applied for the proposed design methods.

5. Conclusions

In this paper the compressive response of S460 and S690 square and rectangular hollow sections has been studied over a wide range of cross-section slendernesses. Test results from 11 concentric stub columns were used for the validation of the developed finite element models. The experimental initial stiffness, ultimate loads and the failure modes were successfully replicated by the finite element models, which were then used to conduct parametric studies. Six aspect ratios and various thicknesses were adopted for both steel grades, thus leading to a $c/t\varepsilon$ varying between 10 and 100. The results

have been used for the assessment of the Eurocode Class 3 slenderness limit, which was found applicable to the currently studied HSS sections, and for the assessment of the design procedures for stocky and slender sections. Regarding the design of slender sections, the application of the Eurocode effective width equations led to largely scattered values. Since Eurocode determines the slenderness of the cross-section on the basis of its most slender element, the effect of the interaction of the constituent plate elements was not taken into account. Element interaction was shown to be pronounced in hollow sections with high cross-section aspect ratios in the slender region. The application of an effective cross-section concept, where the reduction factor is applied on the whole cross-section and is based on the cross-section slenderness rather than on isolated plate elements, was developed and shown to give good results for the currently studied HSS sections, but also for test data collated from literature. For stocky sections in S460, the Eurocode predictions were deemed overly conservative, whilst for cross-sections in S690 which exhibited limited strain-hardening, the Eurocode predictions were appropriate. The applicability of the CSM was therefore extended to S460 hollow sections and was found to lead to safe yet more economic and consistent strength predictions and hence more efficient design. Both proposed design methods were statistically validated according to Annex D of EN 1990 (2002). Further research is needed to generalise the applicability of the design approaches to other HSS grades and facilitate their incorporation in future revisions of EN 1993-1-12.

Acknowledgements

The research leading to these results has received funding from the Research Fund for Coal and Steel (RFCS) under grant agreement No. RFSR CT 2012-00028.

References

AISI S100 (2012) North American specification for the design of cold-formed steel structural members. AISI S100-12 American Iron and Steel Institute.

ANSI/AISC 360-10 (2010) Specification for structural steel buildings. AISC 360–10 Chicago, Illinois: American Institute of Steel Construction.

AS 4100-A1 (2012) Amendment no.1 to AS 4100–1998 steel structures. AS 4100-A1 Sydney, Australia: Australian Standard.

Bock M and Real E (2015) Effective width equations accounting for element interaction for cold-formed stainless steel square and rectangular hollow sections. In Structures 2: 81–90. Elsevier.

Dawson RG and Walker AC (1972) Post-buckling of geometrically imperfect plates. Journal of the Structural Division 98(1): 75–94.

EN 1990 (2002) Eurocode–basis of structural design. Brussels: European Committee for Standardization (CEN).

EN 1993-1-1 (2005) Eurocode 3: design of steel structures. Part 1–1: general rules and rules for buildings. Brussels: European Committee for Standardization (CEN).

EN 1993-1-12 (2007) Eurocode 3: design of steel structures. Part 1–12: additional rules for the extension of EN 1993 up to steel grades S700. Brussels: European Committee for Standardization (CEN).

EN 1993-1-4: 2006+A1 (2015) Eurocode 3: design of steel structures. Part 1–4: general rules – supplementary rules for stainless steels, including amendment A1. Brussels: European Committee for Standardization (CEN).

EN 1993-1-5 (2006) Eurocode 3: design of steel structures. Part 1–5: Plated structural elements. Brussels: European Committee for Standardization (CEN).

Foster ASJ, Gardner L and Wang Y (2015) Practical strain-hardening material properties for use in deformation-based structural steel design. Thin-Walled Structures 92: 115–129.

Galambos TV (1998) Guide to stability design criteria for metal structures. 5th ed. New York: John Wiley & Sons.

Gao L, Sun H, Jin F and Fan H (2009) Load-carrying capacity of high-strength steel box-sections I: Stub columns. Journal of Constructional Steel Research 65(4): 918–924.

Gardner L (2002) A new approach to stainless steel structural design. PhD thesis. Structures Section, Department of Civil and Environmental Engineering, Imperial College London.

Gardner L and Ashraf M (2006) Structural design for non-linear metallic materials. Engineering Structures 28(6): 926–934.

Gardner L and Nethercot DA (2004) Numerical modeling of stainless steel structural components - A consistent approach. Journal of Structural Engineering 130(10): 1586–1601.

Gardner L, Saari N and Wang FC (2010) Comparative experimental study of hot-rolled and cold-formed rectangular hollow sections. Thin-Walled Structures 48(7): 495–507.

Gkantou M, Wang J, Theofanous M, Gardner L and Baniotopoulos C (Submitted) Structural behaviour of high strength steel hollow sections under compression and uniaxial bending. Proceedings of the Institution of Civil Engineers.

Hibbitt, Karlsson and Sorensen Inc ABAQUS (2010) ABAQUS/Standard user's manual volume IIII and ABAQUS CAE manual. Version 6.10. USA: Pawtucket.

Im SW, Kim YS and Chang IH (2005) A study on the characteristics of SM570TMC plates in compression members. Journal of Korean Society of Steel Construction 17(3): 357–363.

Kim DK, Lee CH, Han KH, Kim JH, Lee SE and Sim HB (2014) Strength and residual stress evaluation of stub columns fabricated from 800MPa high-strength steel. Journal of Constructional Steel Research 102: 111–120.

Nishino F, Ueda Y and Tall L (1966) Experimental investigation of the buckling plates with residual stress. Technical report, Fritz Engineering Laboratory Report No. 290.3, Lehigh University, Bethlehem, Pennsylvania, USA.

Rasmussen KJR and Hancock GJ (1992) Plate slenderness limits for high strength steel sections. Journal of Constructional Steel Research 23(1): 73–96.

Sakino K, Nakahara H, Morino S and Nishiyama I (2004) Behavior of centrally loaded concrete-filled steel-tube short columns. Journal of Structural Engineering 130(2): 180–188.

Seif M and Schafer BW (2010) Local buckling of structural steel shapes. Journal of Constructional Steel Research 66(10): 1232–1247.

Shi G, Xu K, Ban H and Lin C (2016) Local buckling behavior of welded stub columns with normal and high strength steels. Journal of Constructional Steel Research 119: 144–153.

Shi G, Zhou W, Bai Y and Lin C (2014) Local buckling of 460 MPa high strength steel welded section stub columns under axial compression. Journal of Constructional Steel Research 100: 60–70.

Su MN, Young B, and Gardner L (2014) Deformation-based design of aluminium alloy beams. Engineering Structures 80: 339–349.

Usami T and Fukumoto Y (1984) Welded box compression members. Journal of Structural Engineering 110(10): 2457–2470.

Wang J, Afshan S, Gkantou M, Theofanous M, Baniotopoulos C and Gardner L (2016) Flexural behaviour of hot-finished high strength steel square and rectangular hollow sections. Journal of Constructional Steel Research 121: 97–109.

Wang J, Afshan S, Schillo N, Theofanous M, Feldmann M and Gardner L (2017) Material properties and compressive local buckling response of high strength steel square and rectangular hollow sections. Engineering Structures 130: 297–315.

Yang D and Hancock GJ (2004) Compression tests of cold-reduced high strength steel sections. I: stub columns. Journal of Structural Engineering 130(11): 1772–1781.

Yoo JH, Kim JW, Yang JG, Kang JW and Lee MJ (2013) Local buckling in the stub columns fabricated with HSA800 of high performance steel. International Journal of Steel Structures 13(3): 445–458.

Yuan B (1997) Local buckling of high strength steel W-shaped sections. Technical report, Open Access Dissertations and Theses, Paper 4059.

Zhou F, Chen Y and Young B (2013a) Cold-formed high strength stainless steel cross-sections in compression considering interaction effects of constituent plate elements. Journal of Constructional Steel Research 80: 32–41.

Zhou F, Tong L and Chen Y (2013b) Experimental and numerical investigations of high strength steel welded H-section columns. International Journal of Steel Structures 13(2): 209–218.

List of Tables

Table 1: Summary of the concentric stub column tests (Wang *et al*., 2017).

Table 2: Comparison of FE and test data.

Table 3: Assessment of design methods for slender sections.

Table 4: Assessment of the effective cross-section method for collated data.

Table 5: Assessment of the continuous strength method for S460 sections with $\bar{\lambda}_{cs} \leq 0.68$.

Table 6: Summary of the reliability analysis for the proposed design methods.

List of Figures

Figure 1: Typical stress–strain curves from tensile flat coupon tests (Wang *et al.*, 2016).

Figure 2: Experimental and numerical load–end-shortening curves for various initial local geometric imperfection amplitudes. a) S460 90×90×3.6; b) S690 90×90×5.6

Figure 3: Typical experimental and numerical failure modes. a) local buckling (S460 90×90×3.6); b) elephant foot (S690 50×50×5)

Figure 4: Typical load–end-shortening curves for S460 RHS with an aspect ratio of 3.00 and various values of plate slenderness

Figure 5: Typical numerical elastic critical buckling mode shapes and failure modes. a) elastic critical buckling mode shapes (SHS, RHS); b) failure modes (SHS, RHS)

Figure 6: Assessment of the European design provisions. a) Class 3 limit for internal elements in compression; b) effective width equations

Figure 7: Proposed effective cross-section method for Class 4 sections. a) determination of coefficients A and B; b) reduction factor ρ_{cs} against $c/t\varepsilon$

Figure 8: Assessment of the continuous strength method for S460 sections with $\bar{\lambda}_{cs} \leq 0.68$. a) $\varepsilon_u/\varepsilon_y$ against cross-section slenderness $\bar{\lambda}_{cs}$; b) assumed material model for the application of the CSM; c) $N_{u,Pred}/N_{u,Test}$ against cross-section slenderness $\bar{\lambda}_{cs}$

Table 1: Summary of the concentric stub column tests (Wang *et al*., 2017).

Cross-section	$N_{u,Exp}$ (kN)	ω_0 (mm)	$\frac{N_{u,Exp}}{Af_y}$
S460 50×50×5	645.16	0.054	1.59
S460 50×50×4	477.63	0.043	1.45
S460 100×100×5	1042.29	0.077	1.14
S460 90×90×3.6	628.34	0.083	1.05
S460 100×50×6.3	1188.45	0.049	1.47
S460 100×50×4.5	713.26	0.070	1.20
S690 50×50×5	804.04	0.076	1.27
S690 100×100×5.6	1673.94	0.081	1.05
S690 90×90×5.6	1511.56	0.089	1.07
S690 100×50×6.3	1409.59	0.106	1.08
S690 100×50×5.6	1212.21	0.156	1.05

Table 2: Comparison of FE and test data.

Cross-section	Imperfection amplitude					
	no imperfection	measured imperfection (ω_0)	Dawson & Walker (ω_{DW})	t/100	t/50	t/10
	$N_{u,FE}/N_{u,Exp}$	$N_{u,FE}/N_{u,Exp}$	$N_{u,FE}/N_{u,Exp}$	$N_{u,FE}/N_{u,Exp}$	$N_{u,FE}/N_{u,Exp}$	$N_{u,FE}/N_{u,Exp}$
S460 50×50×5	0.95	0.93	0.95	0.95	0.93	0.95
S460 50×50×4	0.93	0.89	0.91	0.88	0.85	0.75
S460 100×100×5	1.05	0.96	0.96	0.96	0.96	0.94
S460 90×90×3.6	1.06	1.01	1.01	1.02	1.01	0.99
S460 100×50×6.3	0.99	1.02	1.01	1.01	0.95	0.86
S460 100×50×4.5	0.94	0.97	0.97	0.98	0.94	0.88
S690 50×50×5	0.90	0.90	0.90	0.90	0.90	0.83
S690 100×100×5.6	1.01	1.00	1.00	1.00	1.00	0.98
S690 90×90×5.6	1.00	0.99	1.00	1.00	0.99	0.96
S690 100×50×6.3	1.04	1.01	1.02	1.02	0.99	0.94
S690 100×50×5.6	1.01	0.99	1.00	1.03	1.00	0.97
MEAN	0.99	0.97	0.98	0.98	0.96	0.91
COV	0.05	0.05	0.04	0.05	0.05	0.08

Table 3: Assessment of design methods for slender sections.

Cross-section - Aspect ratio	Effective width equations	Effective cross-section method
	Eqs. (8)-(9)	Proposed Eqs. (10)-(12)
	$\rho_{w,EC3}/\rho_{w,FE}$	$\rho_{cs,Pred}/\rho_{cs,FE}$
H/B=1.00	0.97	0.97
H/B=1.25	0.95	0.96
H/B=1.50	0.94	0.95
H/B=2.00	0.90	0.93
H/B=2.50	0.88	0.95
H/B=3.00	0.85	0.95
MEAN	0.91	0.95
COV	0.07	0.04

Table 4: Assessment of the effective cross-section method for collated data.

Concentric stub columns - Class 4 box cross-sections					
PAPER	Aspect ratio (H/B)	No. of tests	f_y measured (N/mm^2)	$\rho_{cs,Pred}/\rho_{cs,Exp}$ MEAN	$\rho_{cs,Pred}/\rho_{cs,Exp}$ COV
Rasmussen and Hancock (1992)	1.00 (SHS)	2	670	0.94	0.04
Sakino *et al*. (2004)	1.55-2.36 (RHS)	4	540-835	0.98	0.01
Im *et al*. (2005)	1.00 (SHS)	4	533	0.94	0.07
Yoo *et al*. (2013)	1.00 (SHS)	1	761	0.98	0.00

Table 5: Assessment of the continuous strength method for S460 sections with $\bar{\lambda}_{cs} \leq 0.68$.

	FE results (S460)		Experimental results (S460)	
	$N_{u,EC3}/N_{u,FE}$	$N_{u,CSM}/N_{u,FE}$	$N_{u,EC3}/N_{u,Exp}$	$N_{u,CSM}/N_{u,Exp}$
MEAN	0.82	0.97	0.88	0.94
COV	0.17	0.05	0.14	0.08

Table 6: Summary of the reliability analysis for the proposed design methods.

Design method	Reliability analysis parameters					
	n	$k_{d,n}$	$\bar{b}$	V_δ	V_r	γ_{M0}
Effective cross-section method - Proposed Eqs. (10)-(12)	95	3.196	1.050	0.043	0.089	0.960
CSM - Proposed Eq. (17)	73	3.229	1.055	0.056	0.099	0.992

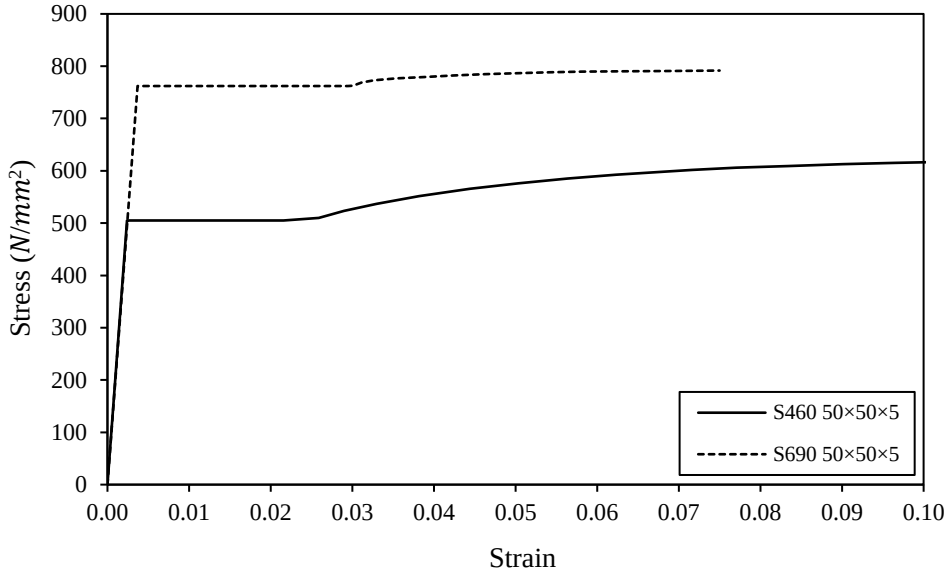

Figure 1: Typical stress–strain curves from tensile flat coupon tests (Wang *et al.*, 2016).

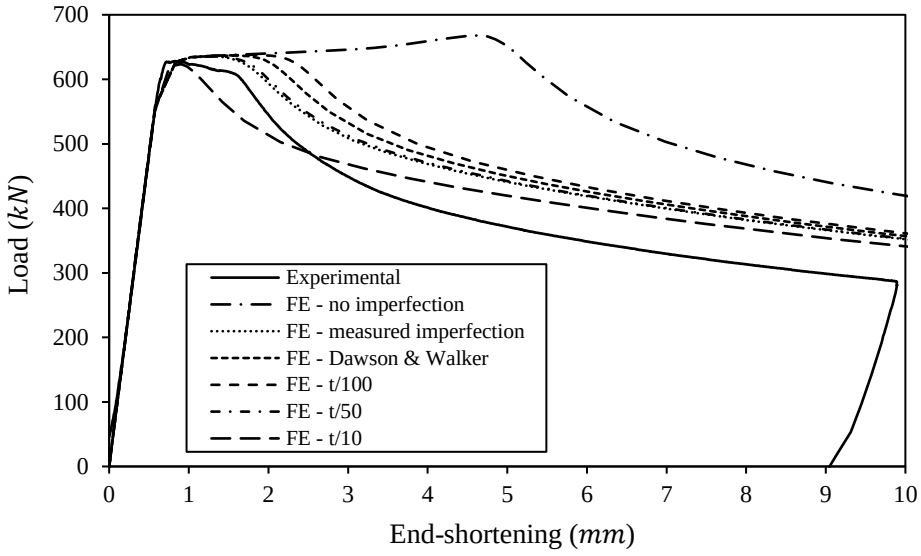

a) S460 90×90×3.6

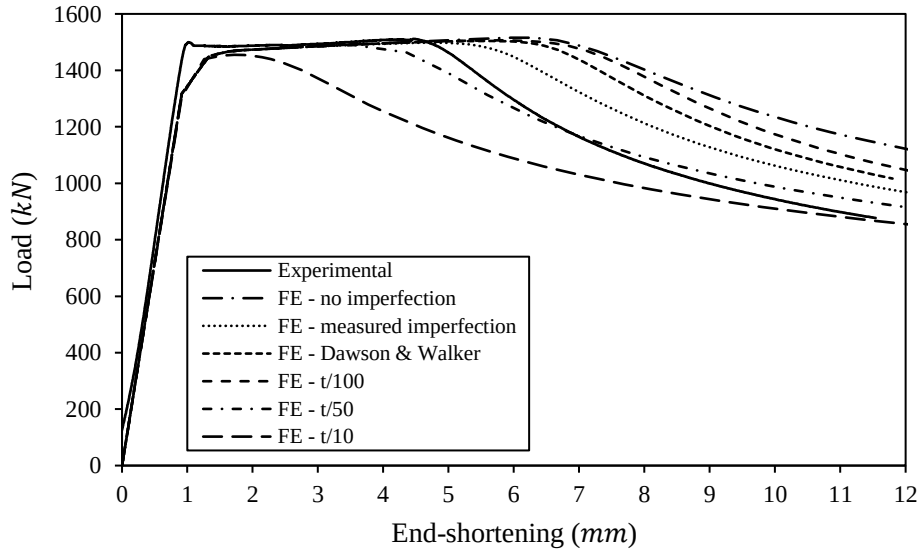

b) S690 90×90×5.6

Figure 2: Experimental and numerical load–end-shortening curves for various initial local geometric imperfection amplitudes.

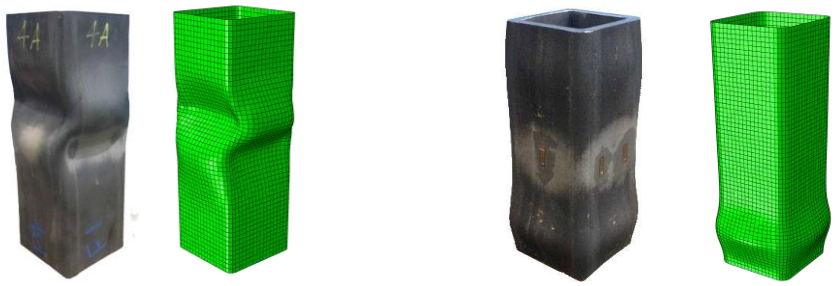

a) local buckling (S460 90×90×3.6) b) elephant foot (S690 50×50×5)

Figure 3: Typical experimental and numerical failure modes.

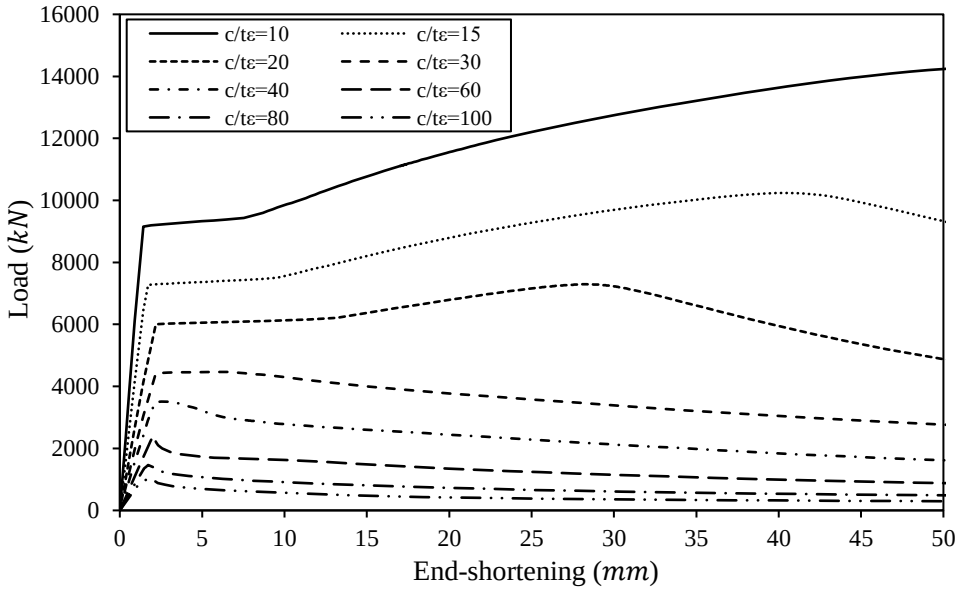

Figure 4: Typical load–end-shortening curves for S460 RHS with an aspect ratio of 3.00 and various values of plate slenderness.

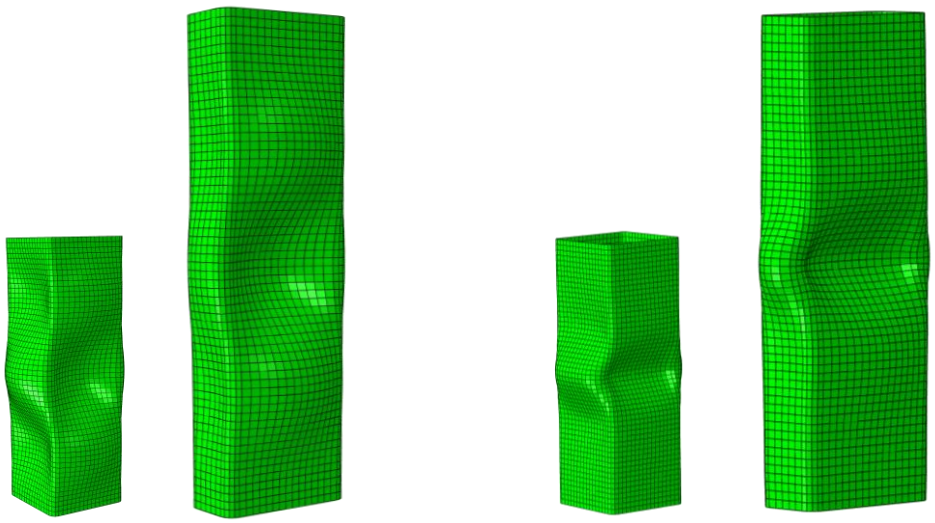

a) elastic critical buckling mode shapes (SHS, RHS)

b) failure modes (SHS, RHS)

Figure 5: Typical numerical elastic critical buckling mode shapes and failure modes.

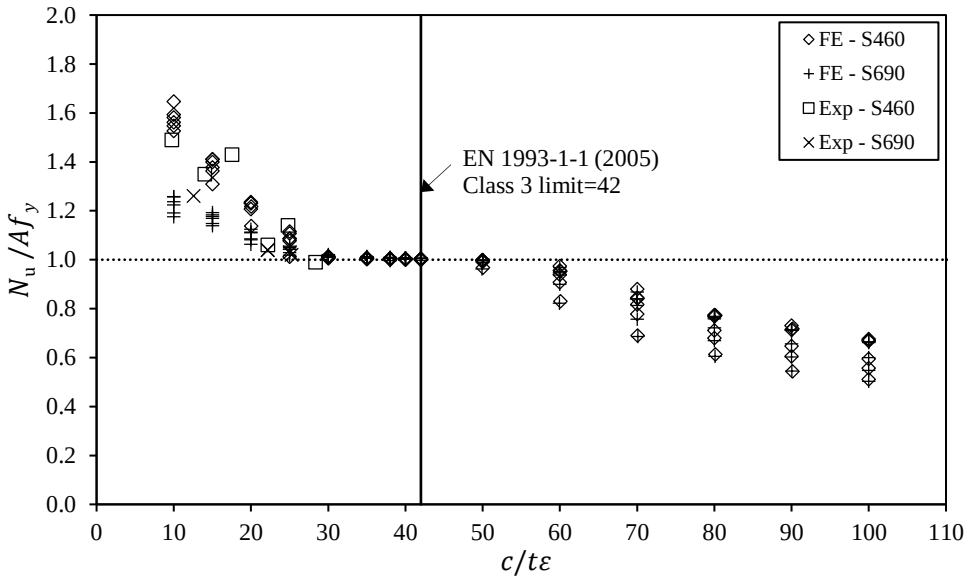

a) Class 3 limit for internal elements in compression

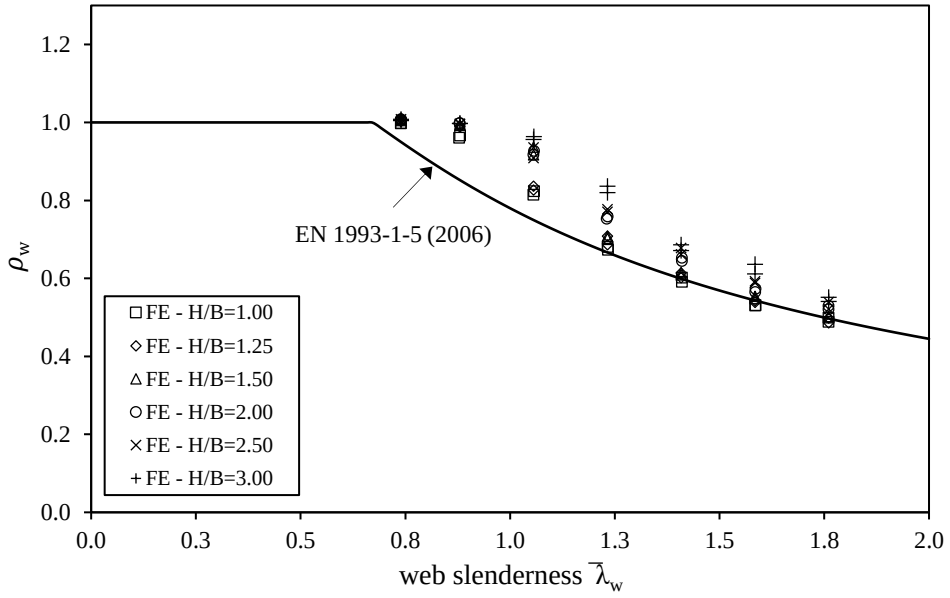

b) effective width equations

Figure 6: Assessment of the European design provisions.

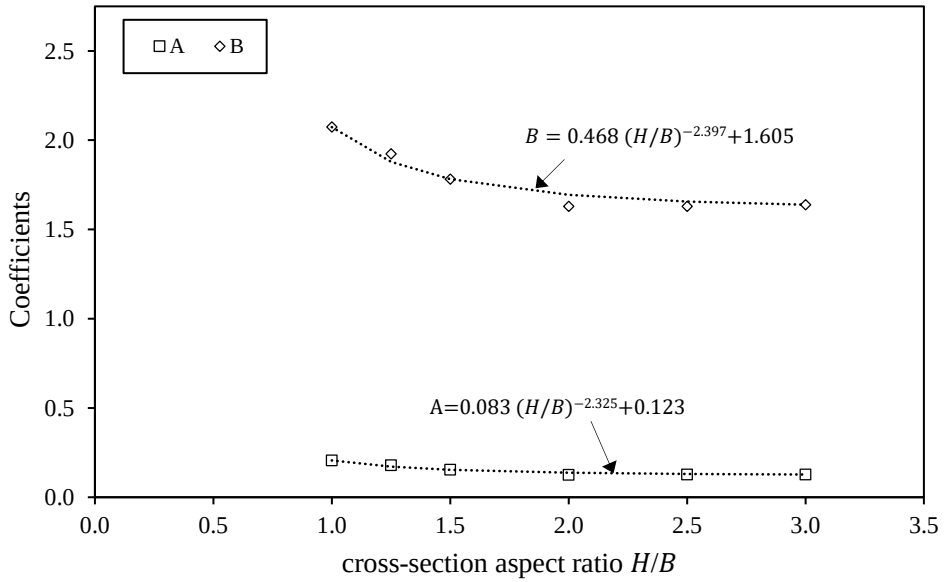

a) determination of coefficients A and B

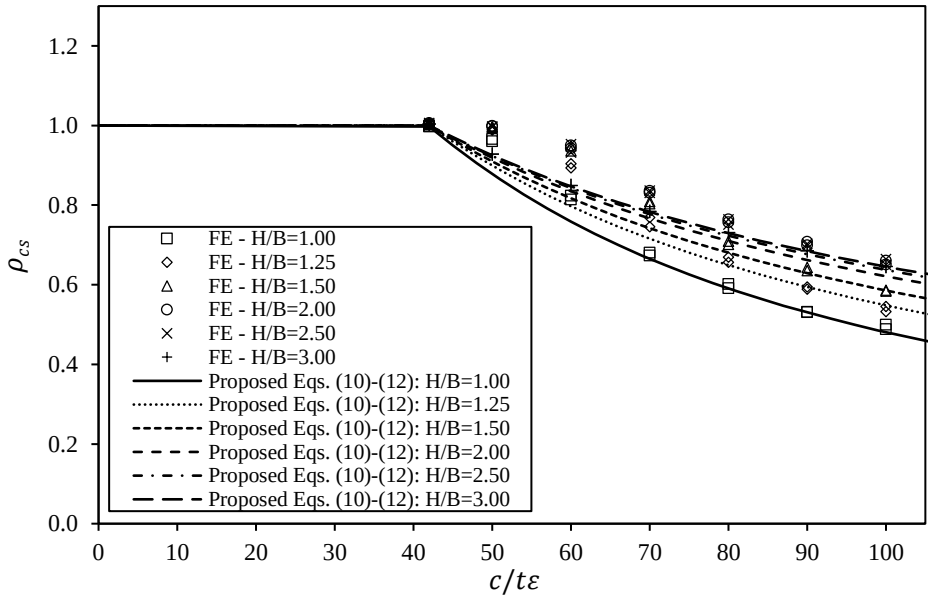

b) reduction factor ρ_{cs} against $c/t\varepsilon$

Figure 7: Proposed effective cross-section method for Class 4 sections.

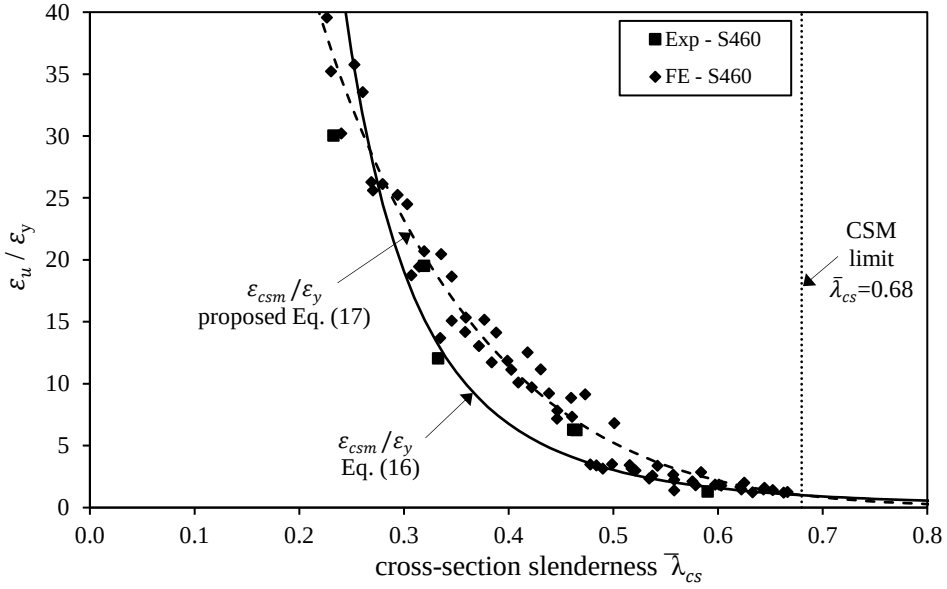

a) $\varepsilon_u/\varepsilon_y$ against cross-section slenderness $\bar{\lambda}_{cs}$

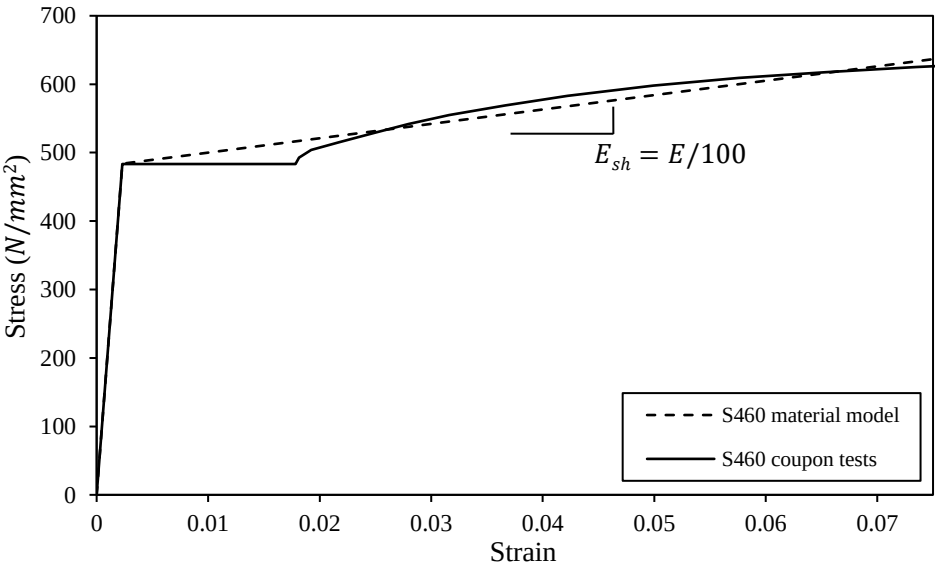

b) assumed material model for the application of the CSM

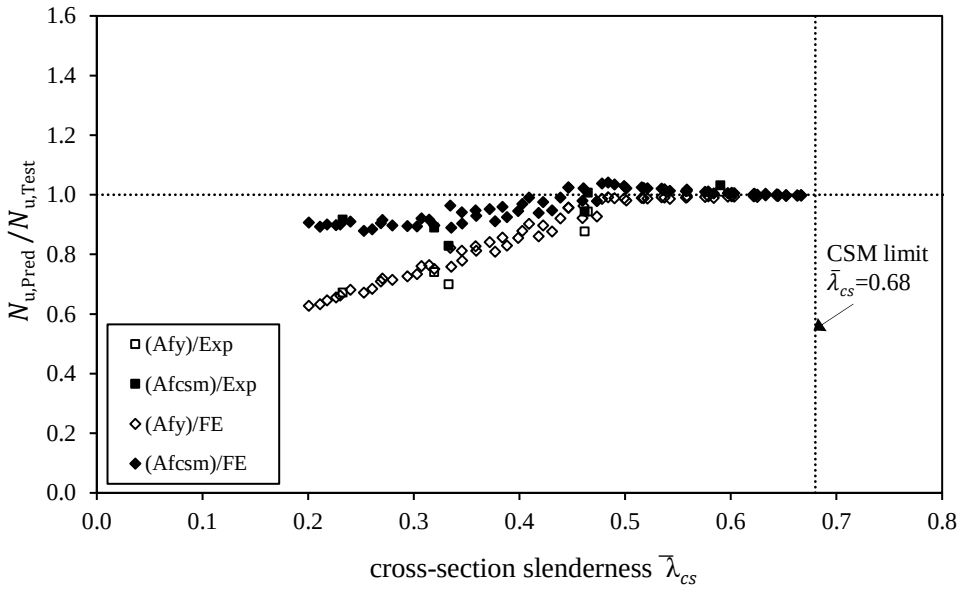

c) $N_{u,Pred}/N_{u,Test}$ against cross-section slenderness $\bar{\lambda}_{cs}$

Figure 8: Assessment of the continuous strength method for S460 sections with $\bar{\lambda}_{cs} \leq 0.68$.

View publication stats